Polymer Journal

REVIEW ARTICLE

Wormlike Micelles of Polyoxyethylene Alkyl Ethers C_iE_j

*By Yoshiyuki EINAGA**

It is demonstrated that wormlike micelles of nonionic surfactants polyoxyethylene alkyl ethers $H(CH_2)_i(OCH_2CH_2)_jOH$ (C_iE_j) have been successfully characterized by static (SLS) and dynamic light scattering (DLS) measurements and viscometry with the aid of the theories developed so far in the field of polymer solution studies, *i.e.*, a molecular thermodynamic theory for light scattering, chain statistical and hydrodynamic theories for semi-flexible polymers. The results for the excess Rayleigh ratio, radius of gyration, hydrodynamic radius, and intrinsic viscosity have been shown to be well represented by the theories based on a wormlike spherocylinder model. Some salient features found for the micelles of C_iE_j with various i or j, their binary mixtures, and the micelles including *n*-alcohol and *n*-alkane are discussed.

KEY WORDS: Wormlike Micelle / Cloud Point Curve / Light Scattering / Radius of Gyration / Hydrodynamic Radius / Intrinsic Viscosity / Polyoxyethylene Alkyl Ether /

The nonionic surfactant polyoxyethylene mono-alkyl ether $H(CH_2)_i(OCH_2CH_2)_jOH$, (abbreviated C_iE_j), exhibits a wide variety of phases in aqueous solution as a function of surfactant concentration and temperature.[1,2] Here, i and j denote the number of methylene groups in the alkyl group and that of repeating units in the oxyethylene group, respectively. At dilute regime, the C_iE_j + water binary system forms an isotropic phase, that is so-called L_1 phase, which consists of micelles formed with the amphiphilic molecules and water. The system exhibits the LCST behavior; the micellar solutions are phase-separated into two phases at high temperatures. It is now well established that the micelles grow in size with increasing concentration and raising temperature, in particular to a greater extent when approaching the phase boundary, assuming threadlike or wormlike cylindrical shape. (See Figure 1.) The wormlike micelles have been visually shown by the cryo-TEM observation,[3] in which in the process of micellar growth, threadlike or polymer-like micelles are evolved in the solutions examined. The micelles are, thus, sometimes called "living" or "equilibrium" polymers in a sense that the linear macromolecules formed can break and recombine.

The polymerlike micelles have certain similarities to real polymers and then their solution properties are analogous to those of real polymer solutions. They have been, thus, rather widely studied to characterize their shape and size by employing the theoretical concepts and experimental methods developped in the polymer solution studies, such as static (SLS) and dynamic light scattering (DLS),[3–12] small-angle neutron scattering (SANS),[13–15] viscometry,[15,16] pulsed-field gradient NMR,[4–7] and so forth. However, solutions of polymer-like micelles are essentially different from those of real polymers. The molar mass of the micelle, *i.e.*, the aggregation number, varies with surfactant concentration, temperature, and other solvent conditions. The average value and distribution of the micellar size are determined by multiple chemical equilibrium among micelles with various aggregation numbers. Although the equilibrium is primarily controlled by the free energy differences among the surfactant molecules located in bulk water, end-capped portion and middle portion of the micelles, it also depends on intermicellar interactions.[17–21] Analyses of scattering data for micellar solutions at finite concentrations are considerably involved, since concentration-dependent intermicellar interactions and micellar growth concomitantly occur in the solutions and the contributions from both effects are not easily decoupled.

For the last several years, we have investigated wormlike micelles of C_iE_j by static (SLS) and dynamic light scattering (DLS) and viscometry.[22–37] In the work, we have been able to determine the concentration-dependent characteristics of the micelles by separating contributions of the intermicellar thermodynamic and hydrodynamic interactions to the SLS and DLS results with the aid of the corresponding theories. We have determined the weight-average molar mass M_w of the micelles as a function of surfactant mass concentration c along with the cross-sectional diameter d from the SLS data by using a molecular thermodynamic theory[21,38] formulated with the wormlike spherocylinder model. It has then found that the molar mass M_w dependence of mean-square radius of gyration $\langle S^2 \rangle$, hydrodynamic radius R_H, and intrinsic viscosity $[\eta]$ for the micelles of pure C_iE_j with various i and j[22–28] and their binary mixtures[29,30] is quantitatively represented by the chain statistical[39] and hydrodynamic theories[40–43] based on the wormlike chain and spherocylinder models, respectively. In particular, it has been demonstrated that the fuzzy cylinder theory[44–47] is favorably applied to analyze the apparent hydrodynamic radius $R_{H,app}$, which is directly obtained from DLS experiment, as a function of the micelle concentration, thereby yielding the concentration-dependent micellar growth

Nishikyouku Ooenishishinbayashicho 6-9-18, Kyoto 610-1141, Japan
*To whom correspondence should be addressed (E-mail: einaga@cc.nara-wu.ac.jp).

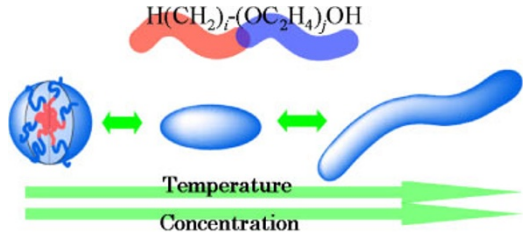

Figure 1. Schematic drawings of the polyoxyethylene alkyl ethers C_iE_j micelle.

by separating contributions of the enhancement of hydrodynamic interactions among micelles with increasing concentration. The analyses have yielded the values of the stiffness parameter λ^{-1} for the micelles. The studies have been extended to the C_iE_j micelles containing *n*-dodecanol, *n*-octanol, and *n*-dodecane in order to explore effects of uptake of *n*-alcohol and *n*-alkane into the micelles on the micellar characteristics.[31–37] The SLS and DLS results were successfully analyzed in a similar fashion to the micelle solutions of single C_iE_j and their binary mixtures.

This review article summarizes characterization and characteristics of the C_iE_j micelles, by mainly focusing on our experimental findings.

CLOUD POINT CURVE

Dilute solutions of C_iE_j micelles are homogeneous at low temperatures but are phase-separated into two phases at higher temperatures above the cloud point curves (*T vs.* wieght fraction *w* curves) shown in Figure 2, in which location and shape of the cloud point curve significantly depend on species of C_iE_j. The phase separation boundary shifts to the lower temperature for the micelle solutions formed with the surfactant of longer hydrophobic or polyethylene chain length *i* and/or of shorter hydrophilic or polyoxyethylene chain length *j*. Accompanying this shift, the cloud point curve is more significantly skewed and the minimum point of the curve (critical point) shift to lower concentrations for larger *i* at fixed *j* or for smaller *j* at fixed *i*.

The phase behavior of the C_iE_j micelle solutions highly resembles that of real polymer solutions in which cloud point curve shifts to lower temperatures and the critical point shift to lower concentrations with increasing molecular weight of the solute polymer when phase separation of the LCST (lower critical solution temperature) type is observed. The above results for the micelle solutions may be, thus, attributed to the fact that wormlike micelles of longer length are formed with C_iE_j molecules of larger *i* at fixed *j* or smaller *j* at fixed *i*. The situations behind the phase diagram of the micellar solutions are, however, more complicated than those for the real polymer solutions, since the length or molar mass of the C_iE_j micelles increases with increasing concentration or with raising temperature.

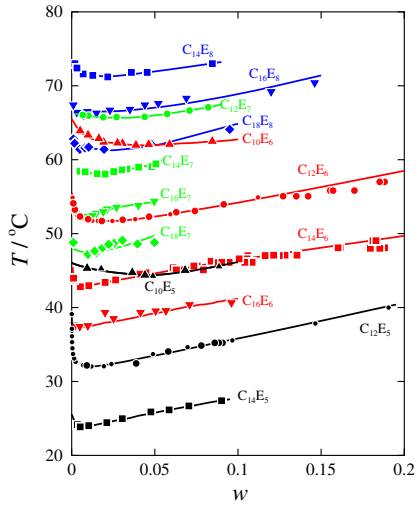

Figure 2. Cloud point curves (temperature *T vs.* weight fraction *w*) for the micelle solutions of various polyoxyethylene alkyl ethers C_iE_j indicated. (cited from Y. Einaga, *Polym. J.*, **39**, 1082 (2007).)

MOLAR MASS OF THE MICELLES

The molar mass and radius of gyration of wormlike micelle is most conveniently determined by SLS measurements on the basis of the fundamental light scattering equation

$$\frac{Kc}{\Delta R_\theta} = \left(\frac{1}{M_w} + 2A_2c + \cdots\right) + \left(\frac{1}{3M_w}\langle S^2\rangle q^2 + \cdots\right) \quad (1)$$

Here, ΔR_θ is the excess Rayleigh ratio at scattering angle θ, M_w is the weight-average molar mass of the micelle, A_2 is the second virial coefficient, $\langle S^2\rangle$ is the z-average radius of gyration of the micelle, K is the optical constant defined by

$$K = \frac{4\pi^2 n^2 (\partial n/\partial c)^2_{T,p}}{N_A \lambda_0^4} \quad (2)$$

with N_A being the Avogadro's number, λ_0 the wavelength of the incident light in vacuum, n the refractive index of the solution, $(\partial n/\partial c)_{T,p}$ the refractive index increment, T the absolute temperature, and p the pressure, and q is the magnitude of the scattering vector defined as

$$q = \frac{4\pi n}{\lambda_0}\sin(\theta/2) \quad (3)$$

In the case of real polymer solutions, the values of M_w, $\langle S^2\rangle$, and A_2 are unequivocally determined by double-extrapolation of $Kc/\Delta R_\theta$ to $\theta \to 0$ and to $c \to 0$ according to eq 1. The technique cannot be applied to micellar solutions, since the size of micelle is concentration-dependent and then M_w, $\langle S^2\rangle$, and A_2 depend on concentration c of the surfactant.

In Figure 3(a) and 3(b), examples of $Kc/\Delta R_0$ *vs.* c plots are exhibitted for solutions of the $C_{12}E_5$ and $C_{12}E_7$ micelles, respectively. The data points at fixed T follow a curve convex downward and the $Kc/\Delta R_0$ value at fixed c decreases with increasing T. These changes reflect not only concentration-dependent micellar growth but concentration-dependent inter-

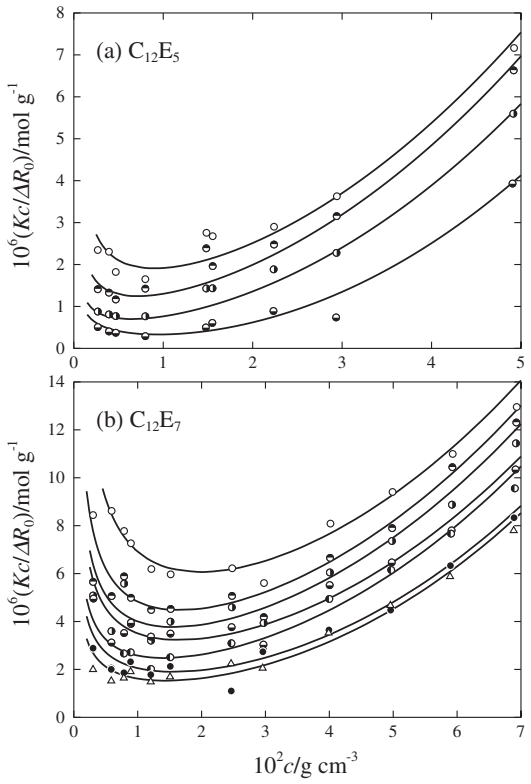

Figure 3. Plots of $(Kc/\Delta R_0)$ against c for the $C_{12}E_5$ (a) and $C_{12}E_7$ (b) micelle solutions at various T: (a) ○, 15.0 °C; ◓, 20.0 °C; ◑, 25.0 °C; ◒, 30.0 °C; (b) ○, 45.0 °C; ◓, 48.0 °C; ◑, 50.0 °C; ◒, 52.0 °C; ◐, 55.0 °C; ●, 58.0 °C; △, 60.0 °C. (cited from ref 26)

micellar interactions. In order to decouple these two effects in the SLS results at a specified concentration, we have to resort to a light scattering theory of micelle solutions. A molecular theory formulated by Sato[21,47] with the wormlike spherocylinder model is useful to this end.

The model consists of a wormlike cylinder of contour length $L - d$ with cross-sectional diameter d and two hemispheres of diameter d which cap both ends of the cylinder, and stiffness of the wormlike cylinder is represented by the stiffness parameter λ^{-1}. (See Figure 4.) In the theory, the weight-average molar mass M_w of the micelles and its distribution have been formulated on the basis of multiple equilibria among various micelles of different sizes and monomer, by representing chemical potentials of the micelles as functions of c in a similar fashion to the classical mean-field and recent molecular theoretical approaches.[19,48,49] In the formulation, the free-energy parameter g_2, which represents the difference in free energy between the surfactant molecules located in the end-capped portion to those in the central cylindrical portion in the micelles, plays a dominant role in the multiple equilibria and then the micellar growth with concentration. The intermicellar thermodynamic interactions have also been taken into account in the chemical potential on the basis of a statistical thermodynamic theory for stiff polymer solutions with the wormlike spherocylinder model.[38] The interactions also affect the micellar growth to some extent, since they may shift the

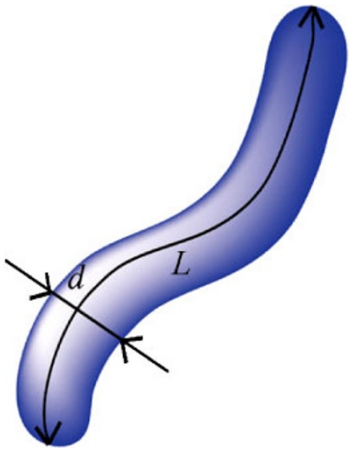

Figure 4. Wormlike spherocylinder model.

multiple equilibria among micelles of various sizes through their chemical potentials. The apparent virial coefficient $A(c)$, which includes the second A_2, third A_3, and higher virial coefficient terms, has been formulated to describe thermodynamic properties of micelle solutions up to high concentrations by taking into account the hard-core repulsive interactions dominated by the parameter d together with the attractive interactions dominated by the parameter $\hat{\epsilon}$ (the depth of the attractive potential well) among the micelles.

The expression for $Kc/\Delta R_0$ is written by

$$\frac{Kc}{\Delta R_0} = \frac{1}{M_w(c)} + 2A(c)c \tag{4}$$

where $M_w(c)$ is the weight-average molar mass of the micelles and $A(c)$ is the apparent second virial coefficient.

Brief summary of the theory may be given as follows: Treatment of the multiple equilibrium conditions among micelles leads to the expression of $M_w(c)$ as:

$$M_w(c) = M_0 N_w = M_0 \left[\frac{(1+\xi)^2 + X}{(1-X)(1+\xi)} \right] \tag{5}$$

with M_0 being the molecular weight of the surfactant molecule and N_w the weight-average aggregation number of the micelle. The quantities X and ξ are defined as:

$$\ln X \equiv (1/N_e)[F_2(N_n, \phi) + g_2 + \ln \phi_e - \ln(N_e/\rho')] \tag{6}$$

$$\xi \equiv (N_e - 1)(1 - X) \tag{7}$$

Here, N_e is the number of surfactant molecules contained in the two hemispheres at the ends of spherocylinder given as

$$N_e = (\pi/6)d^3\rho' \tag{8}$$

where ρ' is the number density of the surfactant molecule in the micelle given by

$$\rho' = N_A/vM_0 \tag{9}$$

with v being the partial specific volume of the micelle. The number-average aggregation number N_n is derived as

$$N_n = (1 + \xi)/(1 - X) \tag{10}$$

In eq 6, ϕ and ϕ_e are the volume fraction of the total micelles in the solution and the equilibrium volume fraction of the smallest micelles, respectively. The former is related to the latter by

$$\phi = \frac{(1+\xi)\phi_e}{(1-X)^2 N_e} \tag{11}$$

and also to c by $\rho = vc$. Function $F_2(N_n, \phi)$ is given by

$$\begin{aligned} F_2(N_n,\phi) = {} & \frac{5}{3}\frac{\phi}{(1-\phi)}\left\{1+\frac{4N_e}{5N_n}\right. \\ & \left.+\frac{2}{5}\left[1+\frac{N_e}{N_n}+\frac{1}{4}\left(\frac{N_e}{N_n}\right)^2\right]\frac{\phi}{(1-\phi)}\right\} \\ & -\ln(1-\phi)+\frac{2}{\pi}\left(2+\frac{N_e}{N_n}\right)\Psi(\hat{\epsilon})\phi \end{aligned} \tag{12}$$

with

$$\Psi(\hat{\epsilon}) = \frac{P^{(1)}[f^{(1)}]^2\hat{\epsilon}}{f^{(1)}-(1/2)f^{(2)}\hat{\epsilon}} \tag{13}$$

and

$$\begin{aligned} f^{(i)} \equiv {} & 1-\frac{\alpha^{(i)}C^{(i)}}{\beta^{(i)}}+\frac{6}{\pi}Q^{(i)}\phi+\frac{\pi C^{(i)}}{6\phi} \\ & \times\left\{1-\exp\left[-\frac{\alpha^{(i)}\phi}{(1/6)\pi\beta^{(i)}-\phi}\right]\right\} \end{aligned} \tag{14}$$

Here, the values of $P^{(i)}$, $Q^{(i)}$, $C^{(i)}$, $\alpha^{(i)}$, and $\beta^{(i)}$ are given in the following Table.[38]

i	$P^{(i)}$	$Q^{(i)}$	$C^{(i)}$	$\alpha^{(i)}$	$\beta^{(i)}$
1	−4.97419	0.487962	1.700943	1.5	$2^{1/2}$
2		−3.98844	−3.19927	2.75	$2^{1/2}$

The apparent virial coefficient $A(c)$ is represented as

$$\begin{aligned} A(c) = {} & \frac{\pi d^3 N_A}{9M_0^2N_e^2}\left[\frac{1+\phi}{(1-\phi)^4}+\frac{3}{2\pi}\Psi(\hat{\epsilon})\right. \\ & \left.+\frac{3}{\pi}\frac{d\Psi(\hat{\epsilon})}{d\phi}\phi+\frac{3}{4\pi}\frac{d^2\Psi(\hat{\epsilon})}{d\phi^2}\phi^2\right] \end{aligned} \tag{15}$$

The values of M_0 and v are known. Thus, we can obtain the X value at given ϕ (or c) by solving eq 6 with the use of eqs 7–14, for a set of values of the parameters d, g_2, and $\hat{\epsilon}$. The X value thus determined allows us to calculate $M_w(c)$ by substituting it into eq 5 along with the values of M_0 and ξ calculated by eq 7. The values of $A(c)$ are calculated by eq 15 as a function of ϕ (or c) for the same set of the values of d and $\hat{\epsilon}$. With the values of $M_w(c)$ and $A(c)$ determined at various ϕ (or c), $Kc/\Delta R_0$ is calculated as a function of c by eq 4. Finally, we can also obtain the weight fraction w_N of the micelles with aggregation number N by

$$w_N = \frac{N(1-X)^2X^{N-N_e}}{1+\xi} \tag{16}$$

As examples, results of the application of eq 4 to the SLS data shown in Figure 3 are depicted in Figures 5 and 6, where $Kc/\Delta R_0$ is double-logarithmically plotted against c. In the analysis, the best-fit theoretical values of $Kc/\Delta R_0$ as a function of c to the experimental data at fixed T have been obtained by selecting the proper values of d, g_2, and $\hat{\epsilon}$, thereby obtaining the $M_w(c)$ values at finite concentrations at each given T. The values of d, g_2, and $\hat{\epsilon}$ are assumed to be independent of T and c. In the figures, the solid and dashed curves represent the calculated values of $Kc/\Delta R_0$ and $1/M_w(c)$, respectively. It is seen that the solid curve for each solution at a given temperature well coincides with the corresponding data points. The good agreement between the calculated and observed results implies that the micelles in dilute aqueous solutions are represented by the wormlike spherocylinder model.

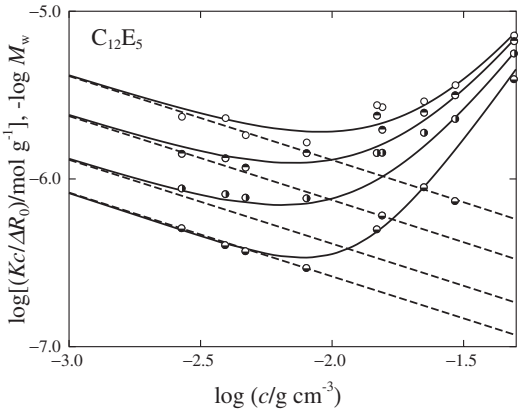

Figure 5. The results of the curve fitting for the plots of $Kc/\Delta R_0$ against c for the $C_{12}E_5$ micelle solutions at various T: Symbols have the same meaning as those in Figure 3(a). The solid and dashed curves represent the calculated values of $Kc/\Delta R_0$ and $1/M_w(c)$, respectively. Temperatures T are 15.0, 20.0, 25.0, and 30.0 °C from top to bottom, respectively. (cited from ref 26)

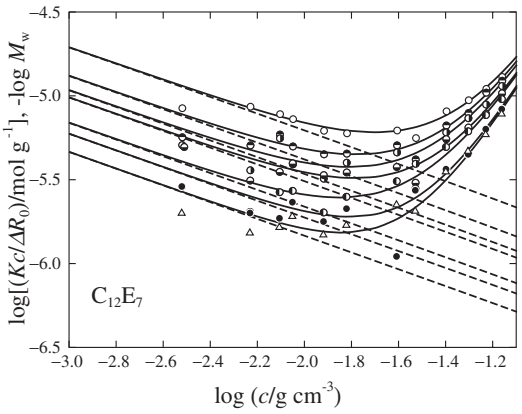

Figure 6. The results of the curve fitting for the plots of $Kc/\Delta R_0$ against c for the $C_{12}E_7$ micelle solutions at various T: Symbols have the same meaning as those in Figure 3(b). The solid and dashed curves represent the calculated values of $Kc/\Delta R_0$ and $1/M_w(c)$, respectively. Temperatures T are 45.0, 48.0, 50.0, 52.0, 55.0, 58.0, and 60.0 °C from top to bottom, respectively. (cited from ref 26)

In Figures 5 and 6, the dashed curve at any fixed T has a slope −0.5, showing that $M_w \propto c^{1/2}$ in the range of c studied. This behavior is in line with the simple theoretical results:

A classical result for the mean contour length $\langle L \rangle$ of polymeric micelles has been derived as

$$\langle L \rangle \simeq \phi^{1/2}\exp(E_{sc}/2k_BT) \tag{17}$$

by the method of mean-field approach such as Flory-Huggins theory.[49,50] Here, ϕ is the surfactant volume fraction, k_B is the Boltzmann constant, and E_{sc} is defined as the energy required to create two hemispherical end caps as the result of scission of a rodlike micelle. Recent treatments[18,19,21,51] of multiple equilibrium between micelles of different sizes and monomers have led for the number-average aggregation number N_n to

$$N_n \propto \phi^{1/2} \exp(\Delta g/k_B T) \tag{18}$$

for highly growing micellar systems. Here, Δg is the micellization free energy which consists of two factors: the difference of the free energy density of threadlike micelle in the end-hemisphere portion to that in the middle-cylinder portion, and the intermicellar interaction terms, that is, excluded volume contributions. In the limit of extensive micellar growth, it is shown that the micellar size distribution becomes the most probable one and then the ratio of the weight-average aggregation number N_w to N_n is equal to 2, without regard to the presence of excluded-volume interactions. It should be noted here that N_w and N_n is related to the weight-average contour length L_w and the number-average L_n, respectively, as described below.

Equation 17 or 18 well represents the observed results in Figures 5 and 6, since $\phi = vc$ and v is substantially approximated to be constant in the range of T and c studied. It indicates that the C_iE_j micelles examined are sufficiently extended according to the theoretical predictions.

The solid and dashed curves coincide with each other at small c and the difference between them steadily increases with increasing c. The results indicate that contributions of the virial coefficients, *i.e.*, the second term of the right hand side of eq 4, to $Kc/\Delta R_0$ are negligible at small c but progressively increase with increasing c as expected. It is seen in Figure 6 that the data points at different T tend to approach with one another as c is increased. The behavior suggests that the thermodynamic properties of the $C_{12}E_7$ micelle solutions may follow the relation $A(c)c \propto c^2$, independent of M_w, predicted for the range of moderately concentrated or semi-concentrate solutions of real polymers.[52,53] It has been found that when the wormlike micelles are sufficiently long, the relation $A(c)c \propto c^2$ is realized at high surfactant concentrations c and the results for rather short micelles exhibit tendency to approach the relation as c is increased.

As typical examples, the values of g_2 and $\hat{\epsilon}$ determined are plotted against T for the $C_{12}E_5$, $C_{12}E_7$, and $C_{14}E_7$ micelles in Figures 7 and 8, respectively. For each micelle, g_2 is an increasing function of T. On the other hand, $\hat{\epsilon}$ does not show clear systematic dependence on the surfactant species, but is roughly constant $\hat{\epsilon}/k_B T \simeq 0.33 \pm 0.03$ except for the one point at the lowest T for the $C_{14}E_7$ micelle solutions. It is found that when compared at fixed T, the g_2 value is larger for the $C_{14}E_7$ micelles than for the $C_{12}E_7$ micelles and that for the $C_{12}E_5$ micelles is larger than that for the $C_{12}E_7$ micelles. Thus, attractive (hydrophobic) interactions among C_iE_j molecules are considered to become stronger with increasing i if j is fixed and with decreasing j if i is fixed. The results are in good

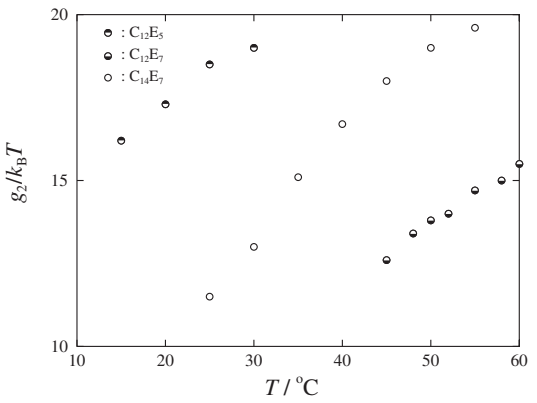

Figure 7. Temperature dependence of g_2 for the $C_{12}E_5$ + water (◓), $C_{12}E_7$ + water (○), and $C_{14}E_7$ + water (◒) systems. (cited from ref 26)

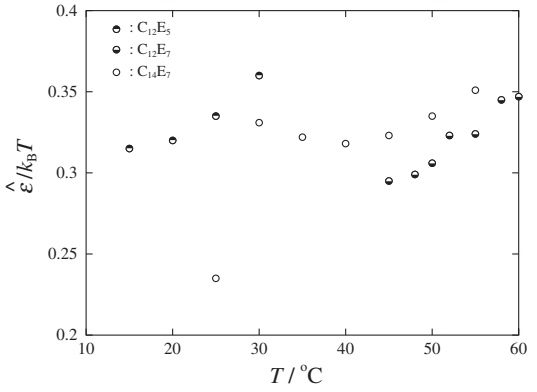

Figure 8. Temperature dependence of $\hat{\epsilon}$ for the $C_{12}E_5$ + water (◓), $C_{12}E_7$ + water (○), and $C_{14}E_7$ + water (◒) systems. (cited from ref 26)

correspondence with those for the molar mass M_w and the length L_w of the C_iE_j micelles as mentioned below.

RADIUS OF GYRATION

According to eq 1, the apparent mean-square radius of gyration $\langle S^2 \rangle_{app}$ at finite concentrations can be determined from the slope of the $Kc/\Delta R_\theta$ *vs.* $\sin^2(\theta/2)$ plot, by using the $M_w(c)$ values determined as described above. Here, we denote $\langle S^2 \rangle$ in eq 1 as $\langle S^2 \rangle_{app}$, since it is possibly affected by intermicellar interactions.

Typical examples of the molar mass M_w dependence of $\langle S^2 \rangle_{app}^{1/2}$ are exhibited in Figure 9 for the $C_{18}E_8$ micelles at various T ranging from 30.0 to 50.0 °C. All the data points form a single composite curve irrespective of temperature and concentration, suggesting that the values of $\langle S^2 \rangle_{app}^{1/2}$ determined at finite c correspond to those for the individual micelles free from inter- and intra-micellar interactions or excluded volume effects. The solid curve shows the best-fit theoretical values of $\langle S^2 \rangle$ calculated for the wormlike chain model by[39]

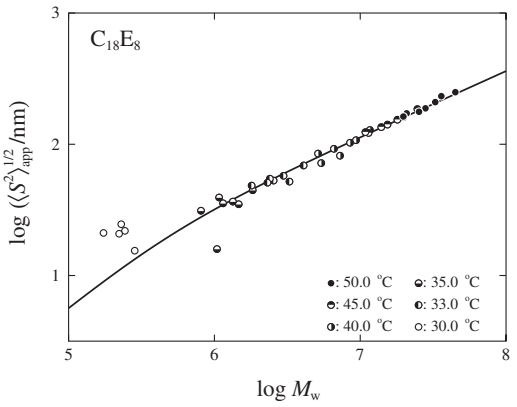

Figure 9. Double-logarithmic plots of $\langle S^2\rangle_{app}^{1/2}$ against M_w. Various symbols represent difference in temperatures: ○, 30.0 °C; ◒, 33.0 °C; ◐, 35.0 °C; ◑, 40.0 °C; ◓, 45.0 °C; ●, 50.0 °C. The solid curve represents the theoretical values calculated by eqs (19) and (20). (cited from ref 23)

$$\lambda^2\langle S^2\rangle = \frac{\lambda L}{6} - \frac{1}{4} + \frac{1}{4\lambda L} - \frac{1}{8\lambda^2 L^2}(1 - e^{-2\lambda L}) \qquad (19)$$

along with the relation

$$L_w = \frac{4\nu M_w}{\pi N_A d^2} + \frac{d}{3} \qquad (20)$$

Here, the relation between L_w and M_w is derived from the micellar volume and L_w is used in place of L in eq 19. In the calculation, the d value obtained in the same way described in the preceding section was used and then the value of λ^{-1} was determined to achieve the best-fit to the observed results. It is found that the calculated results well explains the observed behavior of $\langle S^2\rangle_{app}^{1/2}$. This agreement again shows that the $C_{18}E_8$ micelles assume a wormlike shape.

Similar results have been obtained for all the C_iE_j micelles examined when the value of $\langle S^2\rangle_{app}^{1/2}$ is large enough to be determined by SLS measurements.

INTRINSIC VISCOSITY

In the studies of dilute polymer solutions, intrinsic viscosity $[\eta]$ is usually determined by the extrapolation to zero concentration by Huggins and Fuoss-Mead plots based on the equations

$$\eta_{sp}/c = [\eta] + k'[\eta]^2 c \qquad (21)$$

$$\ln \eta_r/c = [\eta] - \beta[\eta]^2 c \qquad (22)$$

where k' is the Huggins coefficient and β is related to k' by

$$k' + \beta = 1/2 \qquad (23)$$

The usual procedure cannot be, however, applied to the micelle solutions, since the micellar size and hence $[\eta]$ of the micelles decreases with deceasing concentration c. We, thus, have used the following equation to obtain $[\eta]$ at a specified concentration

$$[\eta] = \frac{[2(\eta_{sp} - \ln \eta_r)]^{1/2}}{c} \qquad (24)$$

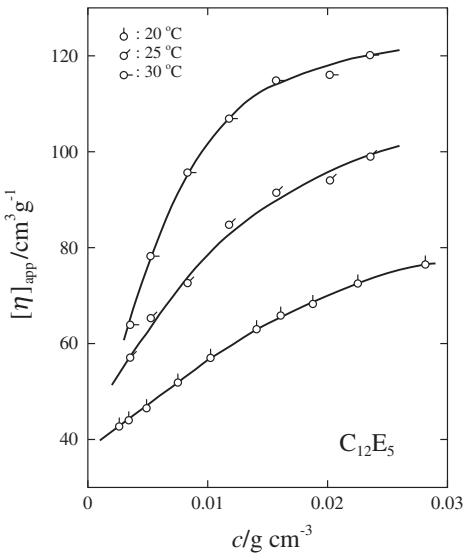

Figure 10. Concentration dependence of the apparent intrinsic viscosity $[\eta]_{app}$ for the $C_{12}E_5$ micelles at various temperatures: Pips with directions of succesive 45° clockwise rotations from pip up correspond to 20.0, 25.0, and 30.0 °C, respectively. (cited from ref 28)

which is derived from eqs 21 and 22 with the relation 23. The symbol $[\eta]_{app}$ is used to denote $[\eta]$ thus determined, since it is uncertain whether or not the concentration ranges of the micelle solutions examined are dilute enough to warrant the validity of eqs 21 and 22.

Examples of concentration dependence of $[\eta]_{app}$ is shown in Figure 10 for the $C_{12}E_5$ micelles. It is found that $[\eta]_{app}$ at fixed temperature increases with c following a curve convex upward. It also increases with raising temperature. The results are considered to come mainly from the fact that the C_iE_j micelles grow in size with increasing concentration and with raising temperature as mentioned above. The increase in $[\eta]_{app}$ with c may, however, possibly reflect the enhancement of the intermicellar hydrodynamic interactions with concentration in addition to the effect of the micellar growth.

In Figure 11, $[\eta]_{app}$ at finite concentrations is double-logarithmically plotted against M_w for $C_{12}E_5$, $C_{12}E_7$, and $C_{14}E_7$ micelles, by using the M_w values determined from the analyses of the SLS data at corresponding concentrations. It is seen that the data points for each micelle at various T and c form a single composite curve, implying that the effects of the intermicellar hydrodynamic interactions on $[\eta]_{app}$ are negligible in the range of c studied. We may interpret the results as indicating that the present $[\eta]_{app}$, though determined at finite concentrations, correspond to $[\eta]$ for the "isolated" micelles formed at given concentrations. We may, thus, analyze the data by using the hydrodynamic theory for wormlike polymers.

The intrinsic viscosity $[\eta]$ for wormlike polymers is formulated by Yoshizaki, *et al.*[43] with the wormlike touched-bead model. The expression for $[\eta]$ has been given as a function of the contour length L or number of beads N, bead

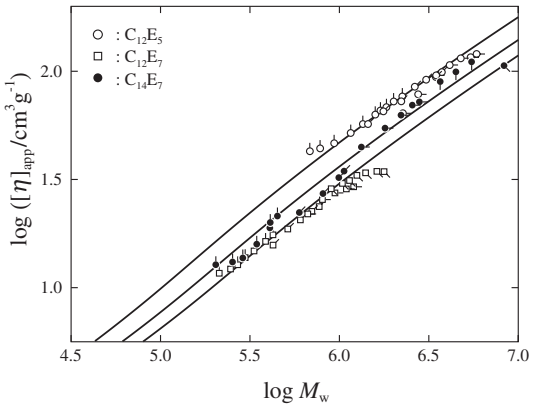

Figure 11. Molecular weight dependence of the apparent intrinsic viscosity $[\eta]_{app}$ for the $C_{12}E_5$, $C_{12}E_7$, and $C_{14}E_7$ micelles: For $C_{12}E_5$ micelles, Pips with directions of succesive 45° clockwise rotations from pip up correspond to 20.0, 25.0, and 30.0 °C, respectively. For $C_{12}E_7$ micelles, Pips with directions of successive 45° clockwise rotations from pip up correspond to 45.0, 50.0, 55.0, and 60.0 °C, respectively. For $C_{14}E_7$ micelles, Pips with directions of succesive 45° clockwise rotations from pip up correspond to 30.0, 35.0, 40.0, 50.0, and 55.0 °C, respectively. The solid curves represent the theoretical values calculated by eqs (19), (20), (25), and (26). (cited from ref 28)

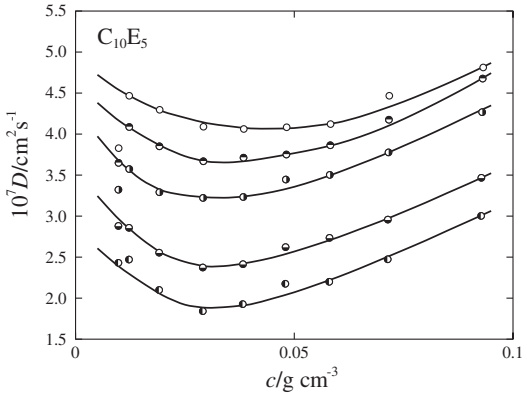

Figure 12. Plots of D against c for the $C_{10}E_5$ solutions at various T: ○, 25.0 °C; ◓, 30.0 °C; ◑, 35.0 °C; ◒, 40.0 °C; ◐, 42.0 °C. (cited from ref 24)

diameter d_b, and stiffness parameter λ^{-1} over the entire range of L including the sphere, *i.e.*, the case $L = d_b$. It reads

$$[\eta] = \frac{6^{3/2}\Phi_\infty \langle S^2\rangle^{3/2}}{M} f_\eta(\lambda L, \lambda d_b) + [\eta]_E \tag{25}$$

$$[\eta]_E = \frac{5\pi N_A N d_b^3}{12M} \tag{26}$$

where the Flory's viscosity coefficient $\Phi_\infty = 2.870 \times 10^{23}$, M is the molecular weight, and $[\eta]_E$ denotes the intrinsic viscosity of the Einstein spheres. It is to be noted that $L = Nd_b$. It has been shown[43] that the values of $[\eta]$ calculated by eq 25 coincide with those calculated with the wormlike cylinder model in the range of large L, if the cross-sectional diameter d of the latter model is taken to be $0.74d_b$; the latter values are available only at large L. We may, thus, calculate $[\eta]$ for the wormlike spherocylinder model by using the relation $d_b = d/0.74$. The expression for the function f_η is so lengthy that we refer it to the original paper.[43]

By eqs 19, 25, and 26, we may calculate $[\eta]$ as a function of M_w by using L_w by eq 20 in place of L and M_w in place of M in these equations and by assigning proper values of the parameters d and λ^{-1}. In Figure 11, the solid lines are best-fit curves to the data points for the corresponding micelles. It is found that the theoretical curves well describe the observed behavior of $[\eta]$. From these curve fittings, we can evaluate the values of d and/or λ^{-1} for the respective C_iE_j micelles. The good agreement between the theoretical and observed results implies that the micelles assume a flexible cylindrical shape which may be represented by the wormlike spherocylinder model. These results are in accordance with the preceding findings from the c dependence of the SLS data and M_w dependence of $\langle S^2\rangle$.

HYDRODYNAMIC RADIUS

In Figure 12, typical examples of the mutual diffusion coefficient D obtained by DLS measurements are depicted as a function of surfactant concentration c for the $C_{10}E_5$ micelle solutions at various temperatures. The data points at fixed T follow a curve concave upward as indicated and the D value at fixed c decreases with increasing T.

The mutual diffusion coefficient D is in general described by[54–56]

$$D = \frac{(1 - \nu c)^2 M}{N_A \zeta}\left(\frac{\partial \pi}{\partial c}\right)_{T,p} \tag{27}$$

where M is the molar mass of the solute, ζ is the translational friction coefficient of the diffusing particle (micelle), and $(\partial\pi/\partial c)_{T,p}$ is the osmotic compressibility. Defining the hydrodynamic radius $R_{H,app}$ (at finite concentrations) according to the Stokes law as

$$\zeta = 6\pi\eta_0 R_{H,app} \tag{28}$$

we obtain

$$D = \frac{(1 - \nu c)^2 M}{6\pi\eta_0 N_A R_{H,app}}\left(\frac{\partial \pi}{\partial c}\right)_{T,p} \tag{29}$$

where η_0 is the solvent viscosity. At infinite dilution, this equation is reduced to the Stokes-Einstein relation

$$D = \frac{k_B T}{6\pi\eta_0 R_{H,app}} \tag{30}$$

Comments on the factor $(1 - \nu c)^2$ in eq 27 may be in order. When the friction coefficient ζ defined in the solvent-fixed frame is used, the diffusion coefficient D in the laboratory-fixed frame (which is relevant to DLS measurements) is related to the concentration gradient $(\partial\mu_0/\partial c)_{T,p}$ at constant T and pressure p of the chemical potential μ_0 of the solvent by the equation including the factor $(1 - \nu c)$ as explicitly given by Berne and Pecora.[54] Then, conversion of $(\partial\mu_0/\partial c)_{T,p}$ to the osmotic compressibility $(\partial\pi/\partial c)_{T,\mu_0}$, which is proportional to

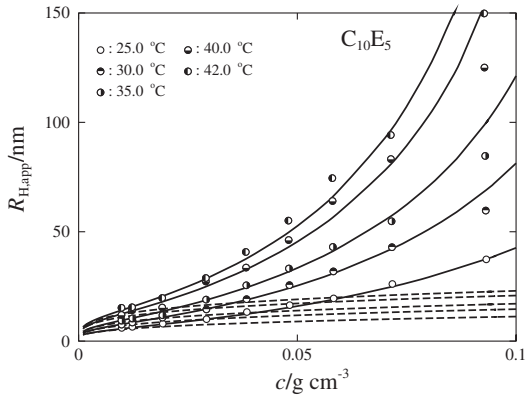

Figure 13. Concentration dependence of $R_{H,app}$ of the $C_{10}E_5$ solutions at various T. The solid and dashed curves represent the calculated values for $R_{H,app}$ by eq (31) and for $R_H(c)$ for the "isolated micelles" by eq (32).

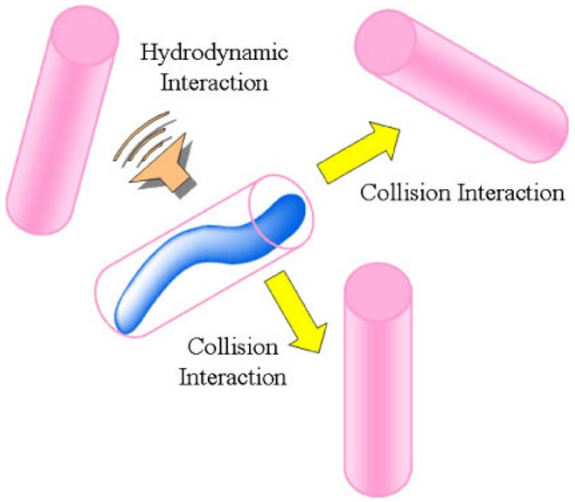

Figure 14. Schematic drawing of the fuzzy cylinder model.

$Kc/\Delta R_0$, arises another factor $(1 - vc)$ as shown by Štěpánek *et al.*[56] The manipulation of the equations, thus, finally results in the factor $(1 - vc)^2$ in the expression of D as given by eq 27. The friction coefficient ζ in this formulation is pertinent to interpret the observed results on the basis of molecular theories, since in most cases ζ is theoretically calculated in the solvent-fixed frame. It is, however, emphasized that eq 27 should be taken as a definition of ζ in a sense and that other expressions of D including the first power of $(1 - vc)$ may be derived when different definition of ζ is employed.

It is understood from eqs 27 and 29 that the results for D as shown in Figure 12 include the concentration-dependent effects of thermodynamic interactions among micelles. We can, however, evaluate $R_{H,app}$ by eq (29) from the DLS data for D and the SLS data for the osmotic compressibility by substituting the values of $M_w(c)$ obtained from the analyses of the corresponding SLS data in place of M, thereby eliminating the thermodynamic effects.

Figure 13 shows the concentration dependence of $R_{H,app}$ calculated by eq 29 from the data in Figure 12 for the $C_{10}E_5$ micelles as an example. It is found that the values of $R_{H,app}$ at fixed c are larger for higher T and $R_{H,app}$ at any given T increases with increasing c. The increase of $R_{H,app}$ does not necessarily correspond to the micellar growth with increasing T and c, *i.e.*, the $R_{H,app}$ values do not necessarily correspond to those for "isolated" micelles. The concentration dependence of $R_{H,app}$ reflects two effects; micellar growth in size and enhancement of the effects of the intermicellar hydrodynamic interactions with increasing c. (See Figure 14.) By taking into account of these effects, we may represent $R_{H,app}$ as a function of c as

$$R_{H,app}(c) = R_H(c)H(c) \tag{31}$$

where $R_H(c)$ represents the hydrodynamic radius of a "isolated" micelle which may grow in size with c and $H(c)$ the hydrodynamic interactions which may be enhanced with c.

In the two functions $R_H(c)$ and $H(c)$, the former may be calculated by employing the equations formulated by Norisuye *et al.*[40] for the wormlike spherocylinder model near the rod limit and by Yamakawa *et al.*[41,42] for the wormlike cylinder model, as a function of the micellar length L with including d and the stiffness parameter λ^{-1}. Their equation for R_H reads

$$R_H = \frac{L}{2f_D(\lambda L, \lambda d)} \tag{32}$$

The expression for the function f_D is so lengthy that we refer it to the original papers.[40–42] We are able to calculate $R_H(c)$ required in eq (31), by combining eq 32 with eq 20, since M_w values as a function of c are obtained from the analyses of the SLS data for the corresponding micelle solutions.

The function $H(c)$ in eq 31 may be calculated with the formulation given by Sato *et al.*[44–46] (see also ref 47) They have recently treated with the concentration dependence of the intermolecular hydrodynamic and direct collision interactions among wormlike polymer chains by using a fuzzy cylinder model. The fuzzy cylinder is defined as a cylinder which encapsulate a wormlike chain or a wormlike spherocylinder in the present case. Its effective length and diameter are evaluated from the wormlike chain parameters L, d, and λ^{-1}. In the fuzzy cylinder theory, Sato *et al.* have taken into account the hydrodynamic interactions among fuzzy cylinders and also jamming effects of the cylinders on the longitudinal and transverse diffusion coefficients along and perpendicular to the chain end-to-end axis, respectively.

Combining Sato *et al.*'s $H(c)$, eq 20, and eq 32 with the experimental results for $M_w(c)$, we may calculate $R_{H,app}(c)$ by eq 31. In Figure 13, the solid curves represent the best-fit theoretical values of $R_{H,app}$ to the observed results calculated by eq 31 by using the d values from the SLS data and selecting the proper values for λ^{-1}. From this fitting, we may evaluate the values of λ^{-1}, *i.e.*, the stiffnes of the micelles. The dashed curves shows the $R_H(c)$ values calculated by eq 32 for the "isolated micelles." From the results in Figure 13, the micellar growth in size with increasing surfactant concentration c is rather moderate and the increase of the apparent hydrodynamic

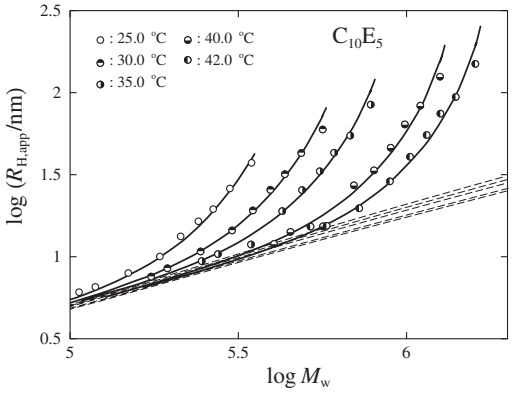

Figure 15. M_w dependence of $R_{H,app}$ of the $C_{10}E_5$ solutions at various T. The solid and dashed curves represent the calculated values for $R_{H,app}$ by eq (31) and for $R_H(c)$ for the "isolated micelles" by eq (32).

radius mainly comes from enhancement of the hydrodynamic and collision interactions among micelles with increasing c.

The same experimantal and calculated results in Figure 13 are shown as double-logarithmic plots of $R_{H,app}$ against M_w in Figure 15. It is seen that as M_w is decreased, *i.e.*, as c is lowered, $R_{H,app}$ of each micelle at fixed T decreases following the curve convex downward shown by the solid line. The theoretical curves for $R_{H,app}$ describe the observed behavior fairly well, implying that the micelles may be represented with the wormlike spherocylinder model. They assymptotically approach the respective dashed lines as M_w (or c) is decreased. The data points at different T also substantially form a single composite curve at low c, or small M_w, implying that the effects of the intermicellar hydrodynamic interactions on $R_{H,app}$ become negligible in the asymptotic region of low c. We note that the dashed curves for the isolated micelles at different T are slightly different from each other. It is also found that the difference between the dashed and solid curves at each T, which steeply increase with M_w, is due to the enhancement of the intermicellar hydrodynamic and dynamic interactions with increasing c, *i.e.*, the contribution of $H(c)$ to $R_{H,app}(c)$.

The substantially same results as those described above are obtained for the other C_iE_j micelles examined.

The λ^{-1} values determined from R_H and/or $[\eta]$ are usually different from those obtained above from the analysis of $\langle S^2 \rangle$ for the same C_iE_j micelles. These differences may be attributed to the fact that there is a distribution in micellar size as shown by eq 16 and different averages are reflected in $\langle S^2 \rangle$ and R_H (and/or $[\eta]$). It has been theoretically shown[19,21] that micelles with sufficiently large aggregation number N have the most probable distribution and the distribution affords a value *ca.* 2 as the ratio of the weight-average aggregation number N_w to the number-average N_n. It is anticipated that the ratio $N_w/N_n = 2$ is realized at the limit of extensive micellar growth, which can be ascertained by the setup of the relation $M_w \propto c^{1/2}$ as examplified in Figures 5 and 6. Thus, the distribution affects the evaluation of λ^{-1} from $\langle S^2 \rangle$, R_H, and $[\eta]$. In the evaluation, the values of λ^{-1} from $\langle S^2 \rangle$ may be most seriously affected by the micellar size distribution, since $\langle S^2 \rangle$ is more significantly dependent on the distribution than R_H and $[\eta]$. Quite recently, Sato and Einaga[47] have shown that the analysis of the micellar length dependence of $\langle S^2 \rangle$ affords the substantially same value of λ^{-1} as that from the analysis of R_H, when the effects of the distribution are taken into accounts by eq 16.

MICELLAR LENGTH

The weight-average micellar length L_w was calculated by eq 20 from the values of $M_w(c)$ and d from the analyses of the SLS data.

The L_w values of the C_iE_5 ($i = 10$, 12, and 14) and $C_{14}E_j$ ($j = 5$, 6, 7, and 8) micelles at three concentrations are plotted against T in Figure 16. It is found that the C_iE_5 micelles grow to a greater length as longer the alkyl chain length i of the surfactant molecules. In this case, the number of the oxyethylene units in the hydrophilic group is fixed to 5 and then the strength in the repulsive force between the adjacent oxyethylene chains may remain constant for different C_iE_5 micelles. On the other hand, attractive force among alkyl

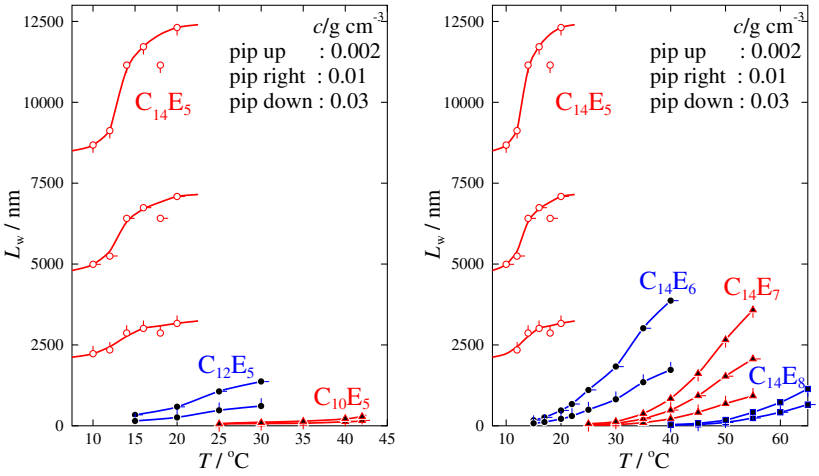

Figure 16. Temperature dependence of L_w for various C_iE_j micelles at indicated concentrations. (cited from ref 27)

chains of the surfactant molecules due to the hydrophobic interactions is considered to become stronger as i is increased. The effects may facilitate the growth of micelles to the greater length for the surfactant C_iE_5 with longer alkyl chain.

As seen in Figure 16, the length L_w of the micelles $C_{14}E_j$ becomes shorter with increasing oxyethylene chain length j. This finding may be interpreted as follows. Since water is a good solvent for polyoxyethylene, the oxyethylene group of the surfactant C_iE_j molecule opt to join the surrounding water molecules, which stabilizes the micelle in water. The affinity among the oxyethylene groups and water molecules causes repulsive force between the adjacent oxyethylene chains on the surface of the micelle, for the one end of the chain is fixed to the micelle core. The repulsive force is considered to be stronger for longer the oxyethylene group and it works to make more surface area of the micelle. This may be the reason why the $C_{14}E_j$ molecules form shorter micelles with increasing j.

As also seen in Figure 16, L_w increases with increasing T. This may be interpreted in the same way as above, *i.e.*, the interactions among the oxyethylene groups of the surfactants and water molecules are reduced and then the force leading to the reduction of the micellar size becomes weaker as temperature is raised. The dependence of the L_w values on T and species of C_iE_j is in good correspondence with that of the parameter g_2 as examplified in Figure 7.

CHARACTERISTICS OF THE C_iE_j MICELLES

Characteristics of the wormlike micelles is given by the values of the parameters d, λ^{-1}, and the spacing s between the hydrophilic tails of adjacent surfactant molecules on the micellar surface. (See Figure 17.)

The d values evaluated from the analyses of the SLS results for various C_iE_j micelles are summarized in Table I, where the column and row represent the alkyl and oxyethylene chain lengths, respectively.

We find that the d value does not significantly vary with hydrophobic and hydrophilic chain length. The results imply that the alkyl and oxyethylene groups of C_iE_j molecules do not take a fully extended or *trans* zig-zag form but assume a randomly coiled form in the micelles. According to the rotational isomeric state (RIS) model calculations by Flory,[57] root mean-square end-to-end distance $\langle R^2\rangle^{1/2}$ of the oxyethylene chains of the C_iE_j molecules listed in the table is *ca.* 1.3 nm. The RIS calculation also gives 1.1–1.4 nm for $\langle R^2\rangle^{1/2}$ of the alkyl chains dependeng on the number of alkyl groups $i = 10$–18. The calculations, thus, give d values of *ca.* 3.7–4.0 nm for the C_iE_j micelles in the table, if it is assumed that the alkyl chains of the surfactant molecules exist in the hydrophobic core in a similar state to the bulk state of amorphous polyethylene and that the oxyethylene chains are oriented straightforwardly in the radial direction from the center line of the cylindrical micelle. The calculated d values are rather large compared with the observed results. The difference suggests that the oxyethylene chains of surfactant molecules are oriented at random on the micellar surface.

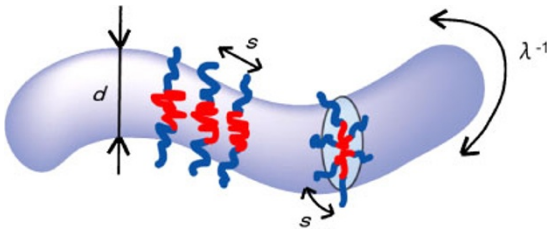

Figure 17. Characteristic parameters of the wormlike micelles.

Table I. Values of the Cross-Sectional Diameter d/nm

	E_5	E_6	E_7	E_8
C_{10}	2.6	2.6		
C_{12}	2.2	2.3	2.4	
C_{14}	2.5	2.4	2.4	2.3
C_{16}		2.5	2.5	2.4
C_{18}			2.5	3.2

Table II. Values of the Stiffness Parameter λ^{-1}/nm

	E_5	E_6	E_7	E_8
C_{10}	35.0	75.0		
C_{12}	12.0	14.0	14.0	
C_{14}	6.0	7.0	13.0	18.0
C_{16}		5.0	6.0	24.0
C_{18}			6.0	25.0

Table III. Values of the Spacing s/nm

	E_5	E_6	E_7	E_8
C_{10}	1.12	1.15		
C_{12}	1.25	1.29	1.33	
C_{14}	1.31	1.30	1.38	1.46
C_{16}		1.31	1.37	1.46
C_{18}			1.41	1.29

Table II summarizes the values of λ^{-1} evaluated from the results for $R_{H,app}$ or $R_H(c)$ by DLS measurements. In this table, we find that λ^{-1} decreases with increasing alkyl chain length i at fixed j except for the C_iE_8 micelles and increases with j at fixed i. This suggests that the relative strength of the repulsive force due to the hydrophilic interaction among C_iE_j molecules in the micelle to the attractive force due to the hydrophobic interactions controls the stiffness parameter; the repulsive force between the adjacent oxyethylene chains contribute to make the micelles stiffer and the attractive force between the adjacent alkyl chains reduce stiffness.

The values of the spacing s are evaluated from the values of d, L_w, and the aggregation number N calculated from M_w. The s values, thus, calculated are summarized in Table III.

The results indicate that the micelles are formed and grow in the way that the hydrophilic groups of the C_iE_j molecules are located at intervals of these s values on the micellar surface on the average. These s values are not significantly different from one another but slightly become larger as the lengths of the alkyl and oxyethylene chains increase, except for the $C_{18}E_8$

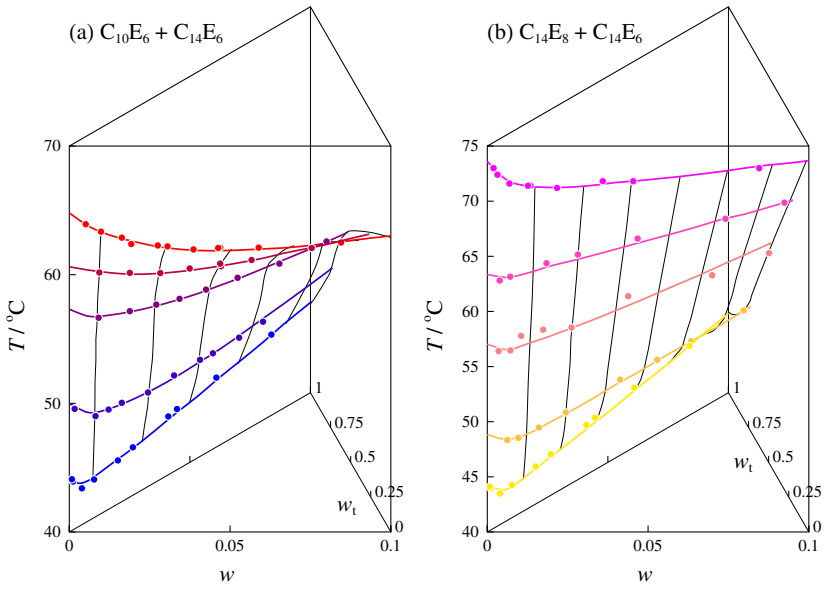

Figure 18. Three-dimensional representation of the binodal surface for micelle solutions of $C_{10}E_6 + C_{14}E_6$ (a) and $C_{14}E_8 + C_{14}E_6$ (b): Circles, observed cloud points. w is the weight fraction of the C_iE_j mixtures in the solution and w_t is the weight fraction of $C_{14}E_6$ in the respective mixtures. (cited from ref 29)

micelle. The above-mentioned RIS values for the end-to-end distance of the oxyethylene chain of the C_iE_j molecules roughly correspond to the observed values of s in the Table III. The RIS calculations may also explain the increase of s with increasing j. The approximate coincidence suggests that the oxyethylene chain of the surfactant molecules is moving by taking a random orientation in water.

WORMLIKE MICELLES OF BINARY C_iE_j MIXTURES

As mentioned above, solution properties, structure, and characteristics of the C_iE_j micelles notably vary with the hydrophobic chain length i and hydrophilic chain length j of the surfactant molecule. They are, thus, considered to depend on the composition of the mixtures when micelles are fomed with mixtures of C_iE_j with different i or j. Figure 18 illustrates the 3D phase diagrams for the aqueous solutions of $C_{10}E_6 + C_{14}E_6$ (a) and $C_{14}E_8 + C_{14}E_6$ (b), where w is the weight fraction of the C_iE_j mixtures in the solution and w_t is the weight fraction of $C_{14}E_6$ in the respective mixtures.

It is seen that all the micelle solutions studied represent the phase separation behavior of the LCST type and that the phase boundaries significantly shift to lower temperatures as w_t increases, or in other word, the component of the larger i increases at fixed j or the component of the smaller j increases at fixed i in the surfactant mixtures. The phase behavior resembles the observations for real polymer solutions, in which the phase boundary of the LCST type is shifted to lower temperatures with increasing polymer molecular weight. Thus, these results suggest that the micellar size becomes larger as the component of the longer hydrophobic chain length or of the shorter hydrophilic chain length increases in the surfactant mixtures.

The micelles formed with binary C_iE_j mixtures are characterized in the same fashion as those of single C_iE_j, by treating the micelle solutions as the binary system which consists of micelles as a solute and water as a solvent.

The weight-average micellar length L_w have been calculated by eq 20 from the values of $M_w(c)$ and d obtained from the analyses of the SLS data. The results at fixed T are shown as functions of c and w_t in Figure 19, in which for all the micelles at a given w_t, L_w becomes larger as c is increased.

As found in Figure 19(a), the micellar length L_w at fixed c steeply increases with increasing w_t, *i.e.*, as the surfactant component with longer alkyl chain length i increases in the surfactant mixtures. This finding may be interpreted as follows: In the surfactant mixtures $C_{10}E_6 + C_{14}E_6$, the number of the oxyethylene units in the hydrophilic group is fixed to 6 irrespective of w_t and then the strength in the repulsive force between the adjacent oxyethylene chains may remain constant for different surfactant mixtures. On the other hand, attractive force among alkyl chains of the surfactant molecules due to the hydrophobic interactions is considered to become stronger as the amount of the component with larger i is increased. The effects may facilitate the growth of micelles to the greater length for this surfactant mixture with increasing the component with longer alkyl chain.

In Figure 19(b), it is seen that the length L_w of the micelles of the mixtures $C_{14}E_8 + C_{14}E_6$ becomes longer with increasing w_t or increasing the component with shorter oxyethylene chain length j at fixed i. Since water is a good solvent for polyoxyethylene, the oxyethylene group of the surfactant C_iE_j molecule is playing a role to stabilize the micelle in water. The affinity among the oxyethylene groups and water molecules causes repulsive force between the adjacent oxyethylene chains on the surface of the micelle, for the one end of the chain is fixed to the micelle core, as stated above. The repulsive force is

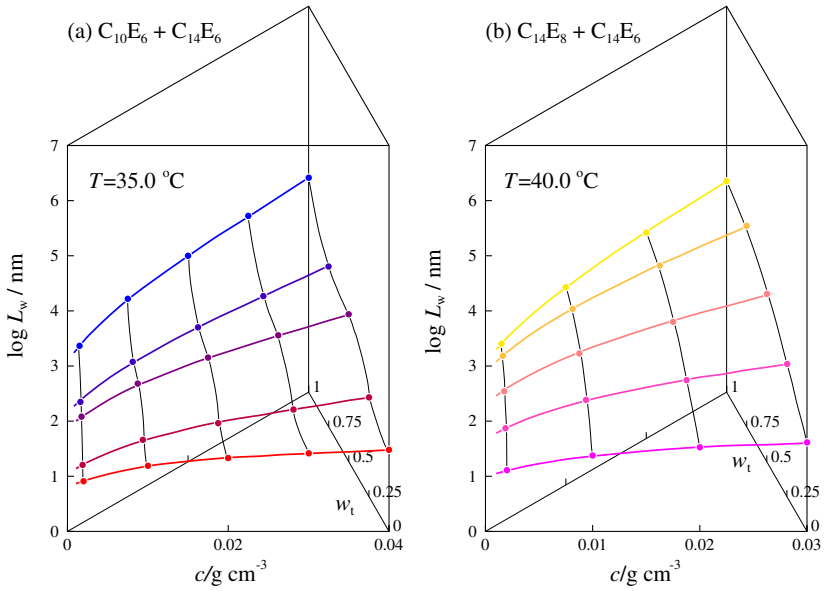

Figure 19. Concentration and w_t dependence of L_w for the micelles of $C_{10}E_6 + C_{14}E_6$ (a) at 35.0 °C and $C_{14}E_8 + C_{14}E_6$ (b) at 40.0 °C. (cited from ref 29)

considered to be stronger for longer the oxyethylene group and it works to make more surface area of the micelle, resulting in the shorter micelles. This may explain the results that the micelles of $C_{14}E_8 + C_{14}E_6$ become longer as the component with smaller j is increased in the surfactant mixtures.

Table IV summarizes the values of d from the SLS results, λ^{-1} from $R_{H,app}$, and s for the micelles formed with binary mixtures $C_{10}E_6 + C_{14}E_6$, $C_{14}E_8 + C_{14}E_6$, $C_{10}E_5 + C_{14}E_5$, $C_{14}E_7 + C_{14}E_5$ at various compositions, where w_t denotes the weight fraction of $C_{14}E_6$ in the binary surfactant mixtures for the former two systems and that of $C_{14}E_5$ in the mixtures for the latter two systems.

We find that the values of the cross-sectional diameter d are almost constant, being independent of the composition w_t. The value of the spacing s doesnot significantly vary with w_t for all the binary mixtures: It slightly increases with increasing w_t for the micelles of the mixtures $C_{10}E_6 + C_{14}E_6$ and $C_{10}E_5 + C_{14}E_5$, and slightly decreases with increasing w_t for those of the mixtures $C_{14}E_8 + C_{14}E_6$ and $C_{14}E_7 + C_{14}E_5$. On the contrary, the stiffness parameter λ^{-1} largely decreases with w_t for the micelles of any system, indicating that the stiffness of the micelle is controlled by the relative strength of the repulsive force due to the hydrophilic interactions between oxyethylene groups to the attractive one due to the hydrophobic interactions between alkyl groups among the surfactant molecules.

The variation of λ^{-1} with oxyethylene chain length due to the change in w_t shows a striking resemblance to the results for regular-comb polymers or polymacromonomers in which the stiffness of the polymers is significantly increased with increasing side-chain length.[58] It has been theoretically shown that the remarkable enhancement of the stiffness is caused by excluded-volume interactions among side chains. Their treat-

Table IV. The Micellar Characteristics

$C_{10}E_6 + C_{14}E_6$ Micelles

w_t	d/nm	λ^{-1}/nm	s/nm
0	2.6	75	1.20
0.250	2.6	27	1.20
0.502	2.5	19	1.23
0.752	2.5	11	1.26
1	2.4	7	1.30

$C_{14}E_8 + C_{14}E_6$ Micelles

w_t	d/nm	λ^{-1}/nm	s/nm
0	2.3	18	1.46
0.246	2.6	17	1.32
0.498	2.6	12	1.31
0.750	2.8	16	1.23
1	2.4	7	1.30

$C_{10}E_5 + C_{14}E_5$ Micelles

w_t	d/nm	λ^{-1}/nm	s/nm
0	2.6	35	1.12
0.247	2.6	32	1.14
0.500	2.4	18	1.20
0.758	2.4	9	1.22
1	2.5	7	1.21

$C_{14}E_7 + C_{14}E_5$ Micelles

w_t	d/nm	λ^{-1}/nm	s/nm
0	2.4	13	1.38
0.251	2.4	12	1.33
0.500	2.4	8	1.30
0.750	2.4	8	1.27
1	2.5	7	1.21

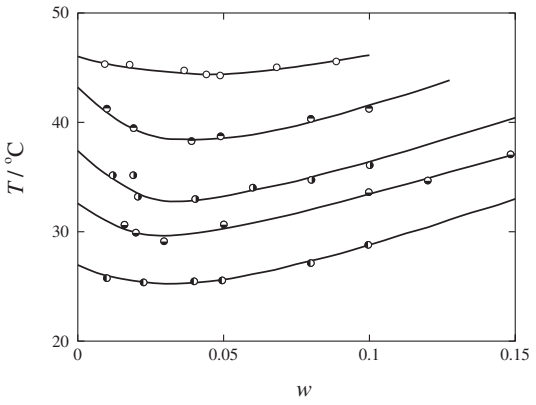

Figure 20. Cloud point curves for the $C_{10}E_5$ + *n*-dodecanol + water system: The weight fraction w_d of *n*-dodecanol in the $C_{10}E_5$ + *n*-dodecanol mixture is 0, 0.0156, 0.0300, 0.0501, and 0.0587 from top to bottom, respectively. (cited from ref 32)

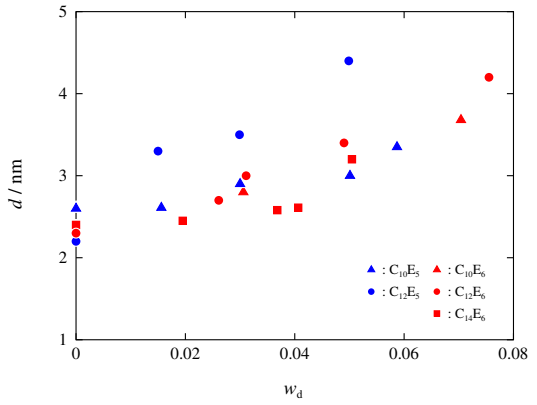

Figure 22. The cross-sectional diameter *d* as a function of w_d for the various C_iE_j micelles containing *n*-dodecanol indicated.

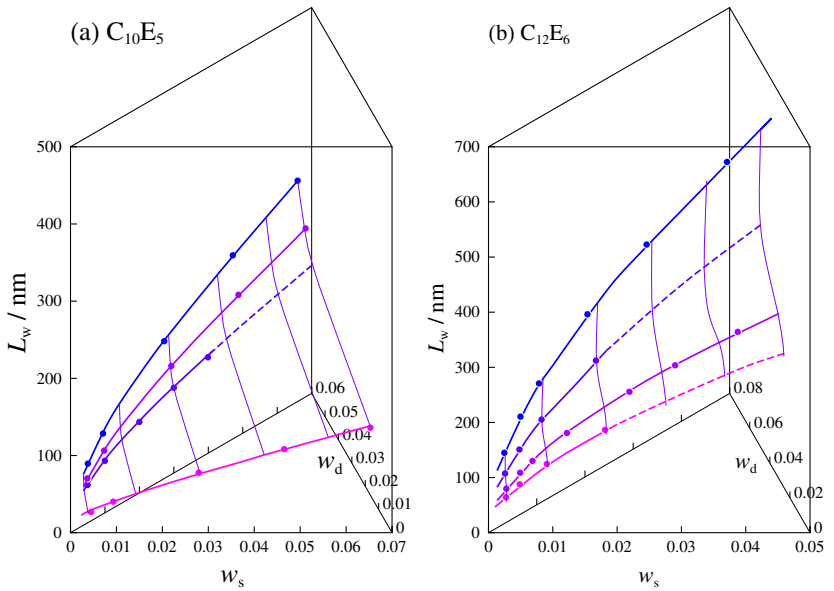

Figure 21. w_s and w_d dependence of the length *L* for the $C_{10}E_5$ + *n*-dodecanol micelles at 20.0 °C (a) and for the $C_{12}E_6$ + *n*-dodecanol micelles at 25.0 °C (b). (cited from ref 32)

ment may also be applied to the present case for the variation of λ^{-1} with oxyethylene chain length. On the other hand, the variation of λ^{-1} with alkyl chain length still remains as a challenging issue.

EFFECTS OF THE UPTAKE OF *n*-ALCOHOL AND *n*-ALKANE

Micelles can, in general, incorpolate an oil such as *n*-alcohol, *n*-alkane, and so forth into (probably) their hydrophobic core. Effects of the uptake of an oil on the properties of micelles have been somewhat extensively studied so far. Aqueous solutions of the surfactant $C_{12}E_5$ containing an oil such as *n*-octane, *n*-decane, and *n*-dodecane were extensively studied[59–67] and it has been found that the surfactant with the oil self-assemble in variety of structures depending on surfactant concentration, oil content, and temperature. In the range of small oil content, $C_{12}E_5$ forms polymer-like or wormlike micelles at low concentrations *c* of the surfactant + oil in the L_1 phase. The micelles grow in length with increasing *c* and the entanglement network is formed in the solution at sufficiently high concentrations. As the oil content is increased, the wormlike micelles are transformed to droplet microemulsions and the bicontinuous microemulsion structures are formed in the solution at high oil content.

Menge *et al.*[59–61] studied the *n*-decane + $C_{12}E_5$ + water system by SLS, DLS, and SANS measurements. They have shown that the apparent molar mass M_{app} of the wormlike micelles formed in the L_1 phase increases with *c* in the range of small *c*, passing through a maximum, and then decreases with increasing *c* at higher *c*. Here, M_{app} includes two contributions, *i.e.*, concentration-dependent molar mass $M_w(c)$ of the micelles

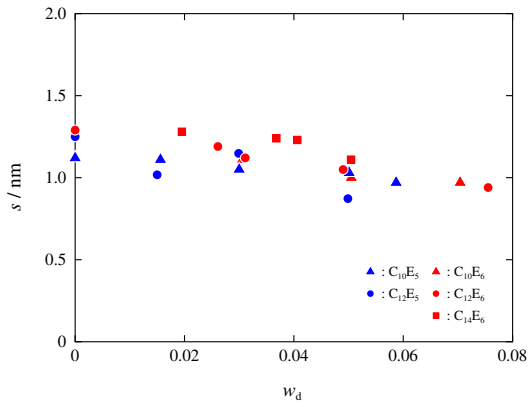

Figure 23. The spacing s of surfactant molecules on the micellar surface as a function of w_d for various C_iE_j micelles containing *n*-dodecanol indicated.

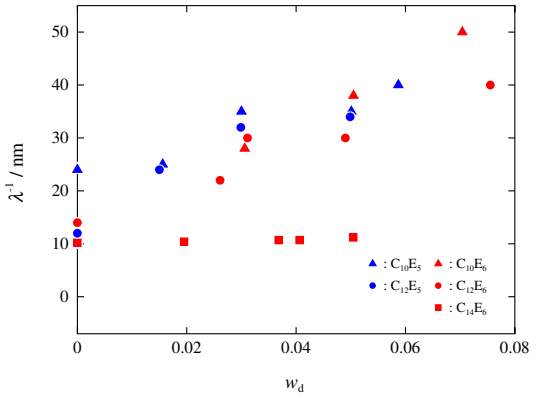

Figure 24. The stiffness parameter λ^{-1} as a function of w_d for various C_iE_j micelles containing *n*-dodecanol indicated.

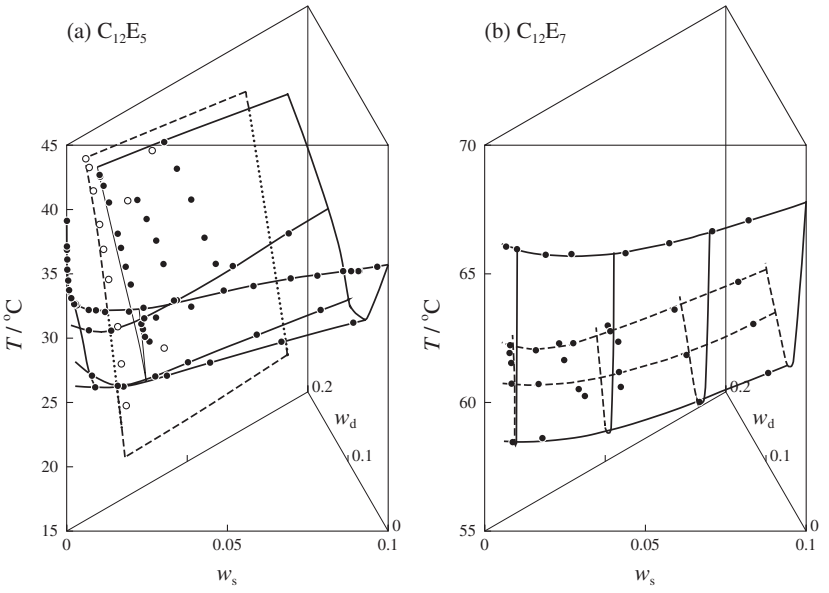

Figure 25. Three-dimensional representation of the phase diagram for the $C_{12}E_5$ + *n*-dodecane + water (a) and $C_{12}E_7$ + *n*-dodecane + water (b) systems: w_s, weight fraction of $C_{12}E_5$ or $C_{12}E_7$ in the respective solution; w_d, weight fraction of *n*-dodecane in the $C_{12}E_5$ or $C_{12}E_7$ + *n*-dodecane mixture. In (a), filled circles and the surface enclosed by the solid lines represent the binodal points and surface, respectively, while the unfilled circles and the surface enclosed by the dashed and dotted lines represent the emulsification failure boundary. In (b), the surface enclosed by the solid and dashed lines represents the binodal surface determined by the cloud points shown by the filled circles. (cited from ref 36)

and concentration dependent structure factor $S(c, q = 0)$ (q the magnitude of scattering vector) which reflects thermodynamic interactions among micelles. The increase of M_{app} at low c, thus, represents the increase of $M_w(c)$, while the decrease of M_{app} at high c is due to dominant contribution of $S(c, q = 0)$ to the SLS results and does not reflect size of the micelles. They have also found that the apparent hydrodynamic radius $R_{H,app}$ as a function of c exhibits a similar behavior to M_{app}. Menge *et al.* have demonstrated the $C_{12}E_5$ micelles in the L_1 phase assume a flexible cylindrical shape and grow in size with increasing c and oil content, although they treat only the apparent quantities obtained by SLS and DLS experiments and have not evaluated $M_w(c)$ and R_H for the micelles by separating the contributions of the thermodynamic and hydrodynamic interactions to the SLS and DLS results.

We have also investigated solution properties of the worm-like micelles of various C_iE_j containing *n*-dodecanol, -octanol, and *n*-dodecane,[32–37] by applying the same technique as in the case of the micelles of C_iE_j and their mixtures described above.

Cloud point curves are shown for the ternary system $C_{10}E_5$ + *n*-dodecanol + water at various w_d in Figure 20, where w and w_d denote the weight fraction of $C_{10}E_5$ + *n*-dodecanol in the solution and that of *n*-dodecanol in the $C_{10}E_5$ + *n*-dodecanol mixture. All the micelle solutions in the figure represent the phase separation behavior of the LCST type and that the phase boundaries significantly shift to lower temperatures as w_d increases. The results again suggest that the micelles grow in size with increasing *n*-dodecanol content.

The weight-average length L_w of the $C_{10}E_5$ and $C_{12}E_6$ micelles containing *n*-dodecanol have been calculated by eq 20

from the values of $M_w(c)$ and d from the analyses of the SLS data. Figure 21 exhibits the results for the former micelles at $T = 20.0\,^{\circ}C$ (a) and for the latter micelles at $T = 25.0\,^{\circ}C$ (b) as functions of the surfactant weight fraction w_s and w_d. Here, w_s is the weight fraction of the surfactant in the solution. For both of the micelles at a given w_d, L_w becomes larger as w_s is increased. As seen in these figures, L_w at fixed w_s steeply increases with increasing w_d, *i.e.*, with uptake of *n*-dodecanol into the micelles. The results are consistent with the finding by Menge *et al.*[59] for the $C_{12}E_5$ micelles containing *n*-decane. Comparing the results in Figure 21(a) and 21(b), we find that L_w of the $C_{12}E_6$ micelles is larger than that of the $C_{10}E_5$ micelles. This is in correspondence with the findings for the C_iE_j micelles discussed above: The longer alkyl group in the surfactant molecule C_iE_j facilitate growth of the micelles due to the stronger hydrophobic or attractive interactions among C_iE_j molecules in the micelle. On the other hand, the longer oxyethylene units depress the micellar growth due to the stronger repulsive interactions among the hydrophilic groups of the adjacent C_iE_j molecules on the micellar surface. The micelles grow in length to the greater extent at higher temperatures. The difference in L_w between the $C_{10}E_5$ and $C_{12}E_6$ micelles containing *n*-dodecanol results from these three competitive effects.

Figure 22 depicts w_d dependence of d for various C_iE_j micelles containing *n*-dodecanol. The d values of these micelles increase with increasing *n*-dodecanol content in the micelles. It is found that they are larger for the $C_{12}E_5$ micelles than for the other C_iE_j micelles at finite w_d. The dependence of the d values on the hydrophobic and hydrophilic chain length is not, however, systematic and thus, we cannot derive definite conclusion about the dependence at present.

The values of the spacing s are plotted against w_d in Figure 23 for various C_iE_j micelles containing *n*-dodecanol. The spacing s value is gradually decreased with increasing w_d for all the micelles, implying that the surfactant molecules are more densely assembled as the *n*-dodecanol content is increased, in order to keep them inside the micelles. We find that it is substantially independent of the hydrophobic and hydrophilic chain length of the surfactant molecules.

Figure 24 illustrates w_d dependence of λ^{-1} evaluated from the analysis of the $R_{H,app}$ *vs.* c plots for the C_iE_j containing *n*-dodecanol indicated. The λ^{-1} values for any of the micelles increase with increasing w_d, except for $C_{14}E_6$ micelles for which λ^{-1} is almost constant irrespective of the w_d value. They are roughly independent of the hydrophobic and hydrophilic chain length of the surfactant molecules with which the micelles are formed. The fact that the micelles become stiffer with uptake of *n*-dodecanol may be correlated with the result that the cross-sectional diameter d of the micelles become larger as *n*-dodecanol content is increased in the micelles.

Figure 25 indicates the 3D phase diagrams for the ternary systems $C_{12}E_5$ + *n*-dodecane + water (panel a) and $C_{12}E_7$ + *n*-dodecane + water (panel b). Here, w_s is the weight fraction of the surfactant $C_{12}E_5$ or $C_{12}E_7$ in the solution, w_d is the weight fraction of *n*-dodecane in the micelle, filled and unfilled

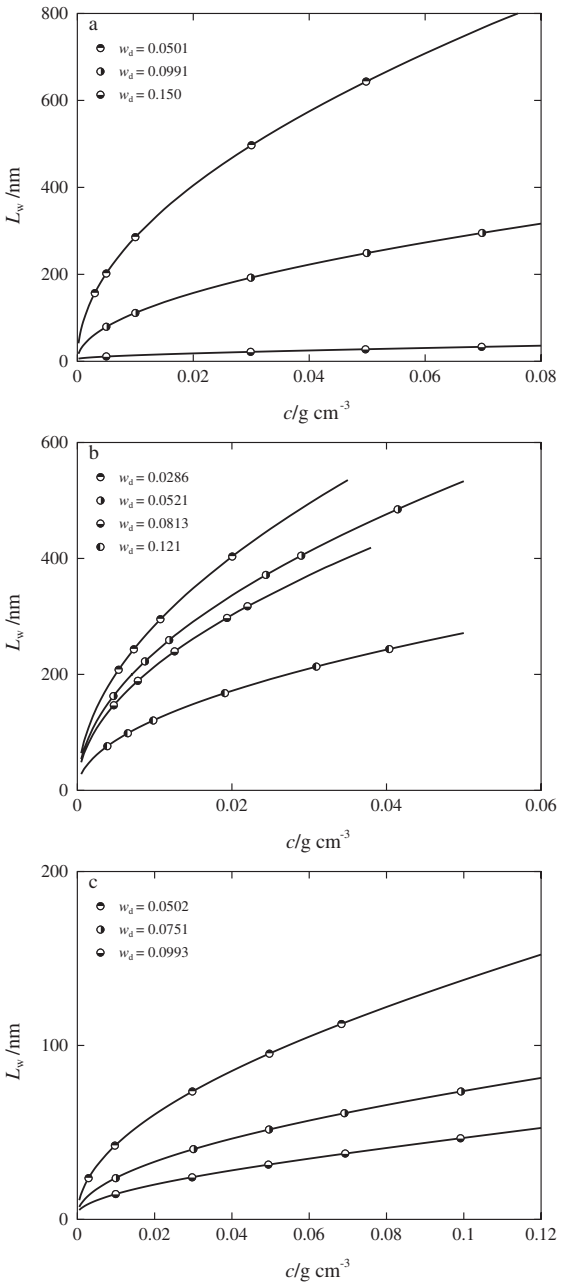

Figure 26. Weight-average micellar length L_w as a function of concentration c for the micelle solutions of $C_{12}E_5$ + *n*-dodecane at 15.0 °C (a), $C_{12}E_6$ + *n*-dodecane at 40.0 °C (b), and $C_{12}E_7$ + *n*-dodecane at 40.0 °C (c) at indicated w_d. (cited from ref 36)

circles represent the cloud points and emulsification failure boundaries, respectively. A series of the data points for the latter near $w_d = 0.028$ are the results by Hellweg and von Klitzing.[67]

We find that at small w_d, the cloud point curve shift to lower temperatures with increasing w_d and then shift to higher temperatures at larger w_d in contrast to the case of the micelle solutions containing *n*-alcohol[31–35] for which the phase boundaries monotonically shift to lower temperatures as the alcohol content increases. In panel a of Figure 25, the emulsification

failure boundary schematically shown by the surface enclosed by dashed and dotted lines indicates that too much *n*-dodecane can not be included in the $C_{12}E_5$ micelles at any T and w_d.

Figure 26 illustrates the weight-average length L_w as a function of the surfactant mass concentration c for the $C_{12}E_5$ + *n*-dodecane micelles at $T = 15.0\,^{\circ}C$ (panel a), for the $C_{12}E_6$ + *n*-dodecane micelles at $T = 40.0\,^{\circ}C$ (panel b), and for the $C_{12}E_7$ + *n*-dodecane micelles at $40.0\,^{\circ}C$ (panel c), respectively. For all the micelles with fixed w_d, the length L_w increases with increasing c.

On the other hand, L_w decreases with increasing *n*-dodecane content w_d contrary to the case of the micelles containing *n*-dodecanol shown above. The former results may indicate that the addition of *n*-dodecane into the micelles weakens hydrophilic interactions among polyoxyethylene tails of the C_iE_j molecules forming micelles and water too significantly to maintain the micellar size as mentioned by Menge *et al.*,[59–61] and leads to collapse of the micelles of smaller size. The latter implies that *n*-alcohol play a role of a kind of co-surfactant in the micelles since it has a hydroxyl group which may work as a hydrophilic group. The decrease of the micellar size with increasing w_d is in correspondence with the the phase behavior shown in Figure 25.

We note that the cross-sectional diameter d and the spacing s as functions of w_d exhibit the same trend as the micelles containing *n*-dodecanol shown in Figures 22 and 23 and the stiffness parameter λ^{-1} is almost independent of w_d.

Received: October 10, 2008
Accepted: November 9, 2008
Published: December 26, 2008

REFERENCES

1. B. Jonsson, B. Lindman, K. Holmberg, and B. Kronberg, "Surfactants and Polymers in Aqueous Solution," John Wiley & Sons, Chichester, 1998.
2. D. J. Mitchell, G. J. T. Tiddy, L. Woring, T. Bostock, and H. T. McDonald, *J. Chem. Soc., Faraday Trans. I.*, **79**, 975 (1983).
3. A. Bernheim-Groswasser, E. Wachtel, and Y. Talmon, *Langmuir*, **16**, 4131 (2000).
4. W. Brown, R. Johnson, P. Stilbs, and B. Lindman, *J. Phys. Chem.*, **87**, 4548 (1983).
5. T. Kato and T. Seimiya, *J. Phys. Chem.*, **90**, 1986 (1986).
6. W. Brown and R. Rymdén, *J. Phys. Chem.*, **91**, 3565 (1987).
7. W. Brown, Z. Pu, and R. Rymdén, *J. Phys. Chem.*, **92**, 6086 (1988).
8. T. Imae, *J. Phys. Chem.*, **92**, 5721 (1988).
9. W. Richtering, W. Burchard, E. Jahns, and H. Finkelmann, *J. Phys. Chem.*, **92**, 6032 (1988).
10. T. Kato, S. Anzai, and T. Seimiya, *J. Phys. Chem.*, **94**, 7255 (1990).
11. T. M. Kole, C. J. Richards, and M. R. Fisch, *J. Phys. Chem.*, **98**, 4949 (1994).
12. H. Strunk, P. Lang, and G. H. Findenegg, *J. Phys. Chem.*, **98**, 11557 (1994).
13. P. Schurtenberger, C. Cavaco, F. Tiberg, and O. Regev, *Langmuir*, **12**, 2894 (1996).
14. G. Jerke, J. S. Pedersen, S. U. Egelhaaf, and P. Schurtenberger, *Langmuir*, **14**, 6013 (1998).
15. O. Glatter, G. Fritz, H. Lindner, J. Brunner-Papela, R. Mittelbach, R. Strey, and S. U. Egelhaaf, *Langmuir*, **16**, 8692 (2000).
16. T. R. Carale and D. Blankschtein, *J. Phys. Chem.*, **96**, 455 (1992).
17. D. Blankschtein, G. M. Thurston, and G. B. Bebedek, *Phys. Rev. Lett.*, **54**, 955 (1985).
18. S. Puvvada and D. Blankschtein, *J. Chem. Phys.*, **92**, 3710 (1990).
19. N. Zoeller, L. Lue, and D. Blankschtein, *Langmuir*, **13**, 5258 (1997).
20. C. B. E. Guerlin and I. Szleifer, *Langmuir*, **15**, 7901 (1999).
21. T. Sato, *Langmuir*, **20**, 1095 (2004).
22. S. Yoshimura, S. Shirai, and Y. Einaga, *J. Phys. Chem. B.*, **108**, 15477 (2004).
23. N. Hamada and Y. Einaga, *J. Phys. Chem. B.*, **109**, 6990 (2005).
24. K. Imanishi and Y. Einaga, *J. Phys. Chem. B.*, **109**, 7574 (2005).
25. Y. Einaga, A. Kusumoto, and A. Noda, *Polym. J.*, **37**, 368 (2005).
26. Y. Shirai and Y. Einaga, *Polym. J.*, **37**, 913 (2005).
27. Y. Einaga, Y. Inaba, and M. Syakado, *Polym. J.*, **38**, 64 (2006).
28. S. Shirai, S. Yoshimura, and Y. Einaga, *Polym. J.*, **38**, 37 (2006).
29. Y. Einaga, Y. Kito, and M. Watanabe, *Polym. J.*, **38**, 1267 (2006).
30. K. Imanishi and Y. Einaga, *J. Phys. Chem. B.*, **111**, 62 (2007).
31. Y. Einaga, Y. Totake, and H. Matsuyama, *Polym. J.*, **36**, 971 (2004).
32. M. Miyake and Y. Einaga, *J. Phys. Chem. B.*, **111**, 535 (2007).
33. M. Miyake and Y. Einaga, *Polym. J.*, **39**, 783 (2007).
34. Y. Einaga, M. Ebihara, and R. Uchida, *Polym. J.*, **39**, 792 (2007).
35. M. Miyake, M. Ebihara, and Y. Einaga, *J. Phys. Chem. B.*, **111**, 9444 (2007).
36. M. Miyake, A. Asano, and Y. Einaga, *J. Phys. Chem. B.*, **112**, 4648 (2008).
37. M. Ochi, S. Matsue, and Y. Einaga, *Polym. J.*, **40**, 442 (2008).
38. R. Koyama and T. Sato, *Macromolecules*, **35**, 2235 (2002).
39. H. Benoit and P. Doty, *J. Phys. Chem.*, **57**, 958 (1953).
40. T. Norisuye, M. Motowoka, and H. Fujita, *Macromolecules*, **12**, 320 (1979).
41. H. Yamakawa and M. Fujii, *Macromolecules*, **6**, 407 (1973).
42. H. Yamakawa and T. Yoshizaki, *Macromolecules*, **12**, 32 (1979).
43. T. Yoshizaki, I. Nitta, and H. Yamakawa, *Macromolecules*, **21**, 165 (1988).
44. T. Kanematsu, T. Sato, Y. Imai, K. Ute, and T. Kitayama, *Polym. J.*, **37**, 65 (2005).
45. A. Ohshima, A. Yamagata, T. Sato, and A. Teramoto, *Macromolecules*, **32**, 8645 (1999).
46. T. Sato, A. Ohshima, and A. Teramoto, *Macromolecules*, **31**, 3094 (1998).
47. T. Sato and Y. Einaga, *Langmuir*, **24**, 57 (2008).
48. D. Blankschtein, G. M. Thurston, and G. B. Benedek, *J. Chem. Phys.*, **85**, 7268 (1986).
49. M. E. Cates and S. J. Candau, *J. Phys. Condens. Matter*, **2**, 6869 (1990).
50. L. J. Magid, *J. Phys. Chem. B*, **102**, 4064 (1998).
51. D. Blankschtein, G. M. Thurston, and G. B. Benedek, *J. Chem. Phys.*, **85**, 7268 (1986).
52. E. F. Casassa and G. C. Berry, in "Comprehensive Polymer Science," G. Allen, Ed., Pergamon Press, New York, 1988.
53. G. C. Berry, in "Soft-Matter Characterization," R. Borsali and R. Pecora, Ed., Springer, Berlin, 2008.
54. B. Berne and R. Pecora, "Dynamic Light Scattering," J. Wiley, New York, 1976.
55. H. Vink, *J. Chem. Soc., Faraday Trans. I.*, **81**, 1725 (1985).
56. P. Štěpánek, W. Brown, and S. Hvidt, *Macromolecules*, **29**, 8888 (1996).
57. P. J. Flory, "Statistical Mechanics of Chain Molecules," John Wiley & Sons, New York, 1969.
58. Y. Nakamura and T. Norisuye, *Polym. J.*, **33**, 874 (2001).
59. U. Menge, P. Lang, and G. H. Findenegg, *J. Phys. Chem. B*, **103**, 5768 (1999).
60. U. Menge, P. Lang, and G. H. Findenegg, *Colloids Surf. A*, **163**, 81 (2000).
61. U. Menge, P. Lang, G. H. Findenegg, and P. Strunz, *J. Phys. Chem. B*, **107**, 1316 (2003).
62. A. Bernheim-Groswasser, T. Tlusty, S. A. Safran, and Y. Talmon,

Langmuir, **15**, 5448 (1999).
63. R. Strey, *Colloid Polym. Sci.*, **272**, 1005 (1994).
64. S. Komura, T. Takeda, Y. Kawabata, S. K. Ghosh, H. Seto, and M. Nagao, *Phys. Rev. E.*, **63**, 41402 (2001).
65. T. Hellweg and D. Langevin, *Phys. Rev. E.*, **57**, 6825 (1998).
66. T. Hellweg and D. Langevin, *Physica A.*, **264**, 370 (1999).
67. T. Hellweg and R. von Klitzing, *Physica A.*, **283**, 349 (2000).

Yoshiyuki EINAGA was born in Himeji, Japan, in 1945, and graduated from the Department of Industrial Chemistry of Kyoto University, Kyoto, Japan in 1967. He studied polymer physics and was awarded Master of Engineering in 1969 and Doctor of Engineering in 1972 at the same university. He recieved a JSPS (Japan Society for the Promotion of Science) Research Fellowship in 1972. He was appointed assistent professor at the Department of Macromolecular Science of Osaka University in 1973. He was a senior research chemist at Carnegie-Mellon University at Pittsburgh in Pennsylvania, USA, from 1979 through 1981. He moved to the Department of Polymer Chemistry of Kyoto University as associate professor in 1988, then to the Department of Chemistry of Nara Women's University as full professor in 1999, and retired from tne university with being awarded the professor emeritus in 2008. His research field is polymer rheology, polymer thermodynamics, solution properties of polymers, and characterization of polymerlike micelles.